Smoothed particle hydrodynamics model for phase separating fluid mixtures. II. Diffusion in a binary mixture

Cedric Thieulot and L. P. B. M. Janssen
Department of Chemical Engineering, Rijksuniversiteit Groningen, Nijenborgh 4, 9747 AG Groningen, The Netherlands

Pep Español
Departamento de Física Fundamental, UNED, Apartado 60141, 28080 Madrid, Spain
(Received 24 November 2004; published 26 July 2005)

A previously formulated smoothed particle hydrodynamics model for a phase separating mixture is tested for the case when viscous processes are negligible and only mass and energy diffusive processes take place. We restrict ourselves to the case of a binary mixture that can exhibit liquid-liquid phase separation. The thermodynamic consistency of the model is assessed and the potential of the model to study complex pattern formation in the presence of various thermal boundaries is illustrated.

DOI: 10.1103/PhysRevE.72.016714 PACS number(s): 02.70.Ns, 05.40.Jc, 05.70.Ln, 83.10.Rs

I. INTRODUCTION

The way a binary mixture phase separates due to purely diffusive processes is an interesting problem by itself. In polymer blends and alloys it is usually a good approximation to neglect viscous processes altogether. Since the pioneering work of Cahn and Hilliard [1] and Allen and Cahn [2], who proposed diffusion processes governed by a Ginzburg-Landau free energy, an impressive amount of work has been done in the field. Several additional phenomena like hydrodynamics and nonisothermal effects have been included, and the formulation of the full set of hydrodynamic equations for phase separating fluids is still a subject of present research. Different theoretical approaches have been taken to derive the continuum equations, among them kinetic theory [3,4], irreversible thermodynamics [5–8], diffuse interface models [9], the general equation for the nonequilibrium reversible-irreversible coupling (GENERIC) approach [10], and projection operators [11].

The resulting equations are complex systems of partial differential equations whose physical content and predictions are best appreciated through numerical simulations. In this respect, many different techniques have been proposed. The most direct are the numerical simulation through finite differences [12,13] or similar usual methods for the numerical solution of the continuum equations. However, other methods have also been used to simulate phase separating fluids, the most popular being the lattice Boltzmann equation [14,15] and the dissipative particle dynamics model [16–18]. With increasing computer power, molecular dynamics simulations capturing the full molecular detail have also been undertaken [19,20].

An overwhelming amount of simulation work has focused on the way a binary mixture phase separates under a sudden temperature quench. In this spinodal decomposition problem different scaling laws for the growth of the separated domains appear depending on the physical mechanisms involved. In a seminal work, Lifshitz and Slyozov described the mechanism in which diffusive exchange of atoms between domains lead to the growth of the larger domains at the expense of the smaller ones [21]. Grant and Elder discuss a hydrodynamic mechanism limiting the growth of domains in viscous fluids and point out the subtleties involved in observing asymptotic regimes in a numerical simulation [22]. A review of the different mechanisms involved in phase separating fluids appears in Ref. [23]. External mechanical forcing on the dynamics of phase separation has also been studied [24]. However, the effects of external thermal gradients on such dynamics is a much underdeveloped field, with a notable exception [25].

In a previous paper [11], we derived from first principles the continuum hydrodynamic equations for a phase separating van der Waals fluid mixture. Ginzburg-Landau models based on an expansion of a free energy up to quartic terms, allows one to get a qualitative picture of phase separation but the contact with actual systems with its molecular specificity is not direct. In order to make the link with molecular detail, it is necessary to look for more detailed equations of state. The van der Waals model for mixtures [26], though being very simple, allows for a more direct connection with systems of experimental interest. In a companion paper [27] we have presented a discrete fluid particle model, which belongs to the family of smoothed particle hydrodynamics models (SPH). What makes the discrete model of Ref. [27] appealing is that, in addition to representing a discretization of the continuum hydrodynamic equations presented in Ref. [11], it is thermodynamically consistent, which means that total mass, momentum, and energy are exactly conserved and that the entropy is a strictly nondecreasing function of time.

The aim of the present paper is to validate the fluid particle model of Ref. [27] by means of numerical simulations for the most simple nontrivial case, which is a diffusive nonisothermal phase separating binary mixture in the absence of viscous processes.

II. THE DISCRETE EQUATIONS

In this section, we particularize the general SPH model of Ref. [27] to the case of a binary mixture when viscous processes can be neglected.

In the absence of viscous processes, the fluid particles remain at rest and they only exchange mass and energy. The state of the system is characterized by $\{N_i^A, N_i^B, U_i\}$ where N_i^A, N_i^B are the number of A and B molecules in a fluid particle and U_i its internal energy. The momentum equation is irrelevant in this case and the governing equations are simply Eqs. (60) and (65) of Ref. [27]. The diffusion and cross-effect transport coefficients $D_i^{\alpha\beta}, S_i^\alpha$ appearing in Eqs. (60) and (65) of Ref. [27] satisfy the following restrictions [11]:

$$m_A S_i^A + m_B S_i^B = 0,$$

$$m_A D_i^{AA} + m_B D_i^{BA} = 0,$$

$$m_A D_i^{AB} + m_B D_i^{BB} = 0,$$

$$D_i^{AB} = D_i^{BA}, \tag{1}$$

where m_A is the mass of a A molecule (idem for B). These restrictions (1) show that only two transport coefficients are independent. We define them as

$$S_i = m_A S_i^A = -m_B S_i^B,$$

$$D_i = m_A^2 D_i^{AA} = m_B^2 D_i^{BB} = -m_A m_B D_i^{AB}. \tag{2}$$

As a consequence of these restrictions (1), the dynamic equations (60) of Ref. [27] imply that the mass of every fluid particle is constant $m_i = m_A N_i^A + m_B N_i^B$, which also means that N_i^A and N_i^B are not independent variables. For the sake of simplicity, we assume that all the fluid particles have the same constant mass $m_i = m$. As all the fluid particles are at rest, the volume $\mathcal{V}_i$ of every fluid particle i, which is defined in terms of the inverse of the density, is also constant. By selecting the particles to be in a regular grid, the volumes of the fluid particles are all identical, and the total mass density is the same for all the fluid particles. In order to reduce the number of parameters to a minimum, we assume that the molecules of both species have the same mass $m_0 = m_A = m_B$. If we introduce the total number of molecules per fluid particle $N_0 = m/m_0$, the invariance of the mass of the fluid particle simply conforms to a condition where the total number of molecules of every fluid particle remains constant, $N_i^A(t) + N_i^B(t) = N_0$. It is convenient to introduce the mass fraction of component A, $x_i = m_A N_i^A / m$ as the independent dynamic variable, so that in the case of equal molecular mass we have

$$N_i^A = N_0 x_i,$$

$$N_i^B = N_0 (1 - x_i). \tag{3}$$

The evolution equations for the independent variables x_i and U_i are obtained from Eqs. (60) and (68) of Ref. [27] after using the definitions (2). They are

$$\begin{aligned} m\dot{x}_i = & \sum_j \frac{F_{ij}}{d_i d_j}(S_i T_i^2 + S_j T_j^2)\left(\frac{1}{T_i} - \frac{1}{T_j}\right) - \sum_j \frac{F_{ij}}{d_i d_j}(D_i T_i \\ & + D_j T_j)\frac{1}{2}\tilde{\tilde{\phi}}_{ij} + \sum_j \frac{F_{ij}}{d_i d_j}\frac{1}{2}(D_i T_i + D_j T_j)(\underset{=i}{\phi} + \underset{=j}{\phi})\left(\frac{1}{T_i} - \frac{1}{T_j}\right) \\ & - \sum_j \frac{F_{ij}}{d_i d_j}(D_i T_i + D_j T_j)\left(\frac{\mu_i}{T_i} - \frac{\mu_j}{T_j}\right), \end{aligned} \tag{4}$$

$$\begin{aligned} \dot{U}_i = & -\sum_j \frac{F_{ij}}{d_i d_j}(D_i T_i + D_j T_j)\frac{1}{2}(\underset{=i}{\phi} + \underset{=j}{\phi})\left(\frac{\mu_i}{T_i} - \frac{\mu_j}{T_j}\right) \\ & + \sum_j \frac{F_{ij}}{d_i d_j}(D_i T_i + D_j T_j)\frac{1}{2}(\tilde{\tilde{\phi}}_i - \tilde{\tilde{\phi}}_j)\left(\frac{\mu_i}{T_i} - \frac{\mu_j}{T_j}\right) \\ & - \sum_j \frac{F_{ij}}{d_i d_j}(S_i T_i^2 + S_j T_j^2)\left(\frac{\mu_i}{T_i} - \frac{\mu_j}{T_j}\right) - \sum_j \frac{F_{ij}}{d_i d_j}\frac{1}{2}(\underset{=i}{\phi} \\ & + \underset{=j}{\phi})\frac{\tilde{\tilde{\phi}}_i - \tilde{\tilde{\phi}}_j}{T_i} + \sum_j \frac{F_{ij}}{d_i d_j}(D_i T_i + D_j T_j)\frac{1}{4}(\underset{=i}{\phi} + \underset{=j}{\phi})^2\left(\frac{1}{T_i} - \frac{1}{T_j}\right) \\ & + \sum_j \frac{F_{ij}}{d_i d_j}(D_i T_i + D_j T_j)\frac{1}{4}(\tilde{\tilde{\phi}}_i - \tilde{\tilde{\phi}}_j)\tilde{\tilde{\phi}}_{ij} - \sum_j \frac{F_{ij}}{d_i d_j}(S_i T_i^2 \\ & + S_j T_j^2)\frac{\tilde{\tilde{\phi}}_i - \tilde{\tilde{\phi}}_j}{T_i} + \sum_j \frac{F_{ij}}{d_i d_j}(\underset{=i}{\phi} + \underset{=j}{\phi})\frac{1}{2}(S_i T_i^2 + S_j T_j^2)\left(\frac{1}{T_i} \\ & - \frac{1}{T_j}\right) + \sum_j \frac{F_{ij}}{d_i d_j}(\kappa_i T_i^2 + \kappa_j T_j^2)\left(\frac{1}{T_i} - \frac{1}{T_j}\right). \end{aligned} \tag{5}$$

In these equations we have introduced the following quantities:

$$\tilde{\phi}_i^\alpha = -\sum_j \sum_\beta (N_i^\beta - N_j^\beta)\bar{\phi}_{ij}^{\alpha\beta},$$

$$\tilde{\tilde{\phi}}_i = \frac{\tilde{\phi}_i^A}{m_A} - \frac{\tilde{\phi}_i^B}{m_B},$$

$$\tilde{\tilde{\phi}}_{ij} = \left(\frac{\tilde{\tilde{\phi}}_i}{T_i} - \frac{\tilde{\tilde{\phi}}_j}{T_j}\right) - \left(\frac{\tilde{\tilde{\phi}}_j}{T_i} - \frac{\tilde{\tilde{\phi}}_i}{T_j}\right),$$

$$\underset{=i}{\phi}^\alpha = -\sum_\beta a_{\alpha\beta} n_i^\beta,$$

$$\underset{=i}{\phi} = \frac{\underset{=i}{\phi}^A}{m_A} - \frac{\underset{=i}{\phi}^B}{m_B},$$

$$\mu_i = \frac{\mu_i^A}{m_A} - \frac{\mu_i^B}{m_B}, \tag{6}$$

and $n_i^\alpha = N_i^\alpha / \mathcal{V}_i$ is the number density of species α. The van der Waals attraction parameter $a_{\alpha\beta}$ is defined in the usual way [11]

$$a_{\alpha\beta} = -\int dr \bar{\phi}^{\alpha\beta}(r). \tag{7}$$

It is convenient to introduce the following parameters [28]:

$$a = \frac{a_{AA} + a_{BB}}{2},$$

$$\Lambda = 1 - \frac{a_{AB}}{a},$$

$$\zeta = \frac{a_{BB} - a_{AA}}{a_{AA} + a_{BB}}. \tag{8}$$

In this way, we can rewrite (6) in terms of the independent variables

$$\tilde{\phi}_i^A = -N_0 \sum_k (x_i - x_k)(\bar{\phi}_{ik}^{AA} - \bar{\phi}_{ik}^{BA}),$$

$$\tilde{\phi}_i^B = -N_0 \sum_k (x_i - x_k)(\bar{\phi}_{ik}^{AB} - \bar{\phi}_{ik}^{BB}),$$

$$\tilde{\tilde{\phi}}_i = -\frac{N_0}{m_0} \sum_k (x_i - x_k)(\bar{\phi}_{ik}^{AA} - 2\bar{\phi}_{ik}^{AB} + \bar{\phi}_{ik}^{BB}),$$

$$\underline{\phi}_i^A = -\frac{N_0 a}{\mathcal{V}_i}[(\Lambda - \zeta)x_i + 1 - \Lambda],$$

$$\underline{\phi}_i^B = -\frac{N_0 a}{\mathcal{V}_i}[-(\Lambda + \zeta)x_i + 1 + \zeta],$$

$$\underset{=i}{\phi} = \frac{N_0 a}{\mathcal{V}_i m_0}(-2\Lambda x_i + \Lambda + \zeta).$$

In all these equations $F_{ij} = F(|\mathbf{r}_i - \mathbf{r}_j|)$ is a positive function defined as

$$\nabla W(r) = -\mathbf{r} F(r), \tag{9}$$

where $W(r)$ is a bell-shaped weight function of finite support and normalized to

$$\int d\mathbf{r}\ W(r) = 1. \tag{10}$$

The density d_i is defined as

$$d_i = \sum_j W(|\mathbf{r}_i - \mathbf{r}_j|). \tag{11}$$

Later in the paper we will specify the actual functional form of the weight function $W(r)$.

Equations (4) and (5) conserve the total energy defined as

$$E(x) = \sum_i U_i - \frac{1}{4} \sum_{ij} \sum_{\alpha\beta} (N_i^\alpha - N_j^\alpha)(N_i^\beta - N_j^\beta)\bar{\phi}_{ij}^{\alpha\beta}. \tag{12}$$

The last term contains the long range part $\bar{\phi}_{ij}^{\alpha\beta} = \bar{\phi}^{\alpha\beta}(r_{ij})$ of the potential of interaction between molecules, evaluated at the distance between different fluid particles r_{ij}. As we have discussed at the end of Ref. [27], we will assume $\bar{\phi}_{ij}^{\alpha\beta} = c_{\alpha\beta} F_{ij}$ where the constant coefficients $c_{\alpha\beta}$ govern the overall intensity of the surface tension effects. Equations (4) and (5) also have the nontrivial, but highly desirable property that the total entropy function defined as

$$S(x) = \sum_i S(\{N_i^\alpha\}, U_i), \tag{13}$$

is a nondecreasing function of time, $\dot{S}(x) \geqslant 0$.

The dynamic equations (4) and (5) must be supplemented with the actual functional forms of the equations of state μ_i and T_i, and the transport coefficients D_i, S_i that can, in principle, depend on the state of the fluid particle i. In the appendix we discuss that a physically reasonable dependence of these transport coefficients is

$$D_i = D_0 x_i (1 - x_i),$$

$$S_i = S_0 x_i (1 - x_i), \tag{14}$$

where D_0, S_0 are constants independent of the thermodynamic state.

Concerning the equations of state, they are obtained from the van der Waals entropy of a fluid mixture, which is given by (see Appendix A of Ref. [27])

$$S(\{N^\alpha\}, U) = k_B \sum_\alpha N^\alpha \left[\frac{D+2}{2} - \ln\left(\frac{n_\alpha \lambda_\alpha^D}{1 - n_0 b} \right) \right]. \tag{15}$$

The thermal wavelength λ_α is defined as

$$\lambda_\alpha = \sqrt{\frac{h^2}{2\pi m_\alpha k_B T}}. \tag{16}$$

Here, h and k_B are the Boltzmann and Planck constants, m_α is the mass of a molecule of species α, and D is the space dimension. The temperature is a function of the extensive variables through

$$k_B T = \frac{2}{D} \frac{1}{N_0} \left(U + \sum_{\alpha\beta} \frac{a_{\alpha\beta}}{V} N^\alpha N^\beta \right). \tag{17}$$

The parameter $b = \Sigma_\alpha n^\alpha b_\alpha / n_0$ is the average excluded volume of the molecules, b_α being the excluded volume of molecules of type α. The parameter $a_{\alpha\beta}$ is the attractive parameter between species α, β.

The derivatives of the entropy with respect to the extensive variables are the intensive variables (or equations of state), i.e., the temperature and the chemical potential,

$$\frac{\partial S}{\partial U} = \frac{1}{T},$$

$$\frac{\partial S}{\partial N_\alpha} = -\frac{\mu_\alpha}{T}. \tag{18}$$

In our case, the temperature is given by (17) and the chemical potential is given by

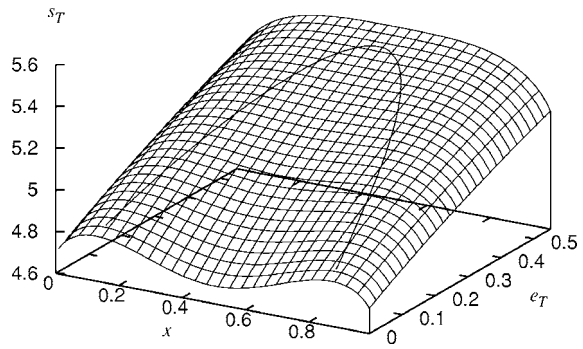

FIG. 1. Three-dimensional plot of van der Waals entropy per molecule $s_T=S_T/N_0$ of the system as a function of the concentration x and the energy per molecule $e_T=E_T/N_0$. The solid line on the surface is the coexistence curve. Magnitudes are in molecular units, as described in Sec. IV.

$$\mu^\alpha = -k_B T\left(\ln\frac{V-bN_0}{\lambda_\alpha^D N^\alpha} - \frac{bN_0}{V-bN_0} + \frac{2\sum_\beta N^\beta a_{\alpha\beta}}{Vk_BT}\right). \tag{19}$$

For the case of a binary mixture where $N^\alpha=N^A,N^B$, we can use the variables N_0,x defined in (3). In this case, the van der Waals entropy (15) becomes

$$S(N_0,x,U) = N_0 k_B\left[\frac{D+2}{2} - \ln\left(\frac{n_0\lambda^D}{1-n_0 b}\right)\right] - N_0 k_B\left[x\ln x + (1-x)\ln(1-x)\right]. \tag{20}$$

Note that if $x=1$ or $x=0$, the van der Waals entropy for a simple fluid is recovered. In Fig. 1 we plot the entropy per molecule S/N_0 defined in (20) as a function of the mass fraction x and the internal energy per molecule $u=U/N_0$. Note the double hump structure characteristic of the van der Waals theory.

We can define the intensive parameters using the variables as

$$\frac{\partial S}{\partial U}(N_0,x,U) = \frac{1}{T},$$

$$\frac{\partial S}{\partial x}(N_0,x,U) = -\frac{m\,\mu}{T}, \tag{21}$$

where now μ is the chemical potential per unit mass (remember that $m=N_0m_0$ is the mass of a fluid particle). In terms of the independent variables, we have the following equations of state:

$$T = \frac{2}{Dk_B}\left(\frac{U}{N_0} + n_0 a[2\Lambda x^2 - 2(\Lambda+\zeta)x + (\zeta+1)]\right),$$

$$\mu = -\frac{k_BT}{m_0}\ln\frac{1-x}{x} - \frac{2n_0a}{m_0}[2\Lambda x - (\Lambda+\zeta)], \tag{22}$$

Note that the chemical potential μ_i defined in Eq. (6) also appearing in the dynamic equations (4) is precisely the same one defined above.

III. THE EQUILIBRIUM STATE

The dynamic equations (4) and (5) conserve the total energy, the total number of molecules of species A and the total mass of every fluid particle m_0N_0. In addition, they ensure that the total entropy is a monotonously increasing function of time. As a consequence, the dynamic equations (4) and (5) have a final equilibrium state x^{eq} that maximizes the total entropy subject to the conservation of the energy and the number of molecules of species A. In terms of the dynamic variable x_i, the total number of molecules of species A is $N_0^A(x)=N_0m_0\Sigma_i x_i$. In order to obtain the equilibrium state, we maximize without any restriction the following function:

$$S(x) - \frac{1}{T_0}[E(x) - \mu_0 N_0^A(x)], \tag{23}$$

where T_0 and μ_0 are suitable Lagrange multipliers. The maximum of the function (23) occurs at the equilibrium value x^{eq} which, in principle, will be a function of T_0,μ_0. The actual values of T_0,μ_0 are obtained by requiring that $x^{\mathrm{eq}}(T_0,\mu_0)$ fulfills the constraints

$$\sum_i U_i = E_0,$$

$$N_0\sum_i x_i = N_0^A, \tag{24}$$

where E_0 is the total energy of the system and N_0^A is the total number of molecules of species A in the system. Note that in Eq. (24) we assumed that there are no surface tension terms in the energy, just for the sake of simplicity. The maximization of the function (23) leads to the following set of equations, one for each fluid particle:

$$\frac{\partial S}{\partial U_i} = \frac{1}{T_0},$$

$$\frac{\partial S}{\partial x_i} = \frac{\mu_0}{T_0}. \tag{25}$$

We can rewrite these equations simply by using the definitions (22) for the intensive parameters,

$$T(x_i^{\mathrm{eq}},U_i^{\mathrm{eq}}) = T_0,$$

$$\mu(x_i^{\mathrm{eq}},U_i^{\mathrm{eq}}) = \mu_0. \tag{26}$$

The above equations simply state that the equilibrium state is such that all the fluid particles have the same temperature and chemical potential. The solution of the coupled set of equations (26) provides the equilibrium state $U_i^{\mathrm{eq}},x_i^{\mathrm{eq}}$ of Eqs. (4) and (5) that is reached as time tends towards infinity. On

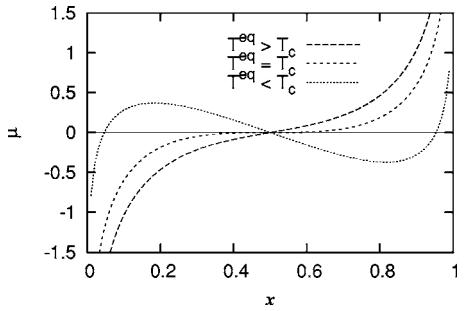

FIG. 2. Representation of the chemical potential μ as a function of the concentration for different temperatures. Magnitudes are in molecular units, as described in Sec. IV.

the other hand, the chemical potential $\mu(x)$ is defined as being the difference between μ^A and μ^B [27] and we know that the chemical potentials for each component in a mixture tend towards a unique value at equilibrium [29], leading us to expect $\mu(x_i^{\mathrm{eq}}, U_i^{\mathrm{eq}})=0$. By considering Eq. (22), the equilibrium value of the concentration x_i^{eq} is the solution of the equation

$$k_B T^{\mathrm{eq}} \ln \frac{1-x_i^{\mathrm{eq}}}{x_i^{\mathrm{eq}}} + 2n_0 a\Lambda(2x_i^{\mathrm{eq}}-1) = 0, \tag{27}$$

where we have assumed $a_{AA}=a_{BB}$, this is $\zeta=0$ for the sake of simplicity. The curve $T^{\mathrm{eq}}=f(x_i^{\mathrm{eq}})$ is the coexistence curve. The critical point is defined by the coordinates

$$x_i = \frac{1}{2}, \quad T_c = \frac{\Lambda a n_0}{k_B}, \tag{28}$$

above which constituents A and B form a homogeneous solution regardless of their concentration.

In Fig. 2 the chemical potential in Eq. (22) is plotted for different values of the ratio T^{eq}/T_c. If $T^{\mathrm{eq}}>T_c$ we observe that the equation $\mu(x_i^{\mathrm{eq}}, U_i^{\mathrm{eq}})=0$ has a unique solution $x=1/2$. If on the other hand, $T^{\mathrm{eq}}<T_c$, then two additional solutions appear, symmetrical with respect to $x=1/2$. Due to the dependence of T_c on Λ, it is obvious that this is only valid if $\Lambda>1$, which means that when molecules of equal type attract each other with greater force than those of unequal type, phase separation may occur.

IV. SIMULATION SETUP

We perform numerical simulations of the dynamic equations (4) and (5). N_T fluid particles are arranged in a regular two-dimensional lattice with periodic boundary conditions. In this way, the volume of every fluid particle is exactly the same. The first order differential equations are integrated with a fourth-order Runge-Kutta algorithm. Every fluid particle interacts with their neighbors according to the range h of the weight function $W(r)$. We select as the weight function the Lucy function defined by

$$W(r) = \frac{5}{\pi h^2}\left(1+3\frac{r}{h}\right)\left(1-\frac{r}{h}\right)^3 \tag{29}$$

which is normalized to unity in 2D [30].

We recall in what follows the large set of parameters that enter into the model and make suitable selections in order to limit the scope of this very rich model. The first set of parameters are of molecular nature and appear in the equations of state. These are the mass of the molecules, m_α, the excluded volumes of both species b_α, the attraction parameters $a_{\alpha\beta}$, and the parameters $c_{\alpha\beta}$ controlling surface tension. In order to keep the number of parameters to a minimum, we assume that the mass of the molecules of both species is the same, i.e., $m_A=m_B=m_0$. Also, the excluded volume of both species is assumed to be equal, $b_A=b_B=b$ as well as the attraction parameters $a_{AA}=a_{BB}=a$. This means that the parameters defined in Eq. (8) become

$$\Lambda = 1 - \frac{a_{AB}}{a}, \quad \zeta = 0. \tag{30}$$

In this paper, we will limit ourselves to the case $\Lambda=1$ which means that there is absolutely no attraction between molecules of different species. Although physically unlikely, we expect this to favor phase separation when it is expected to occur.

The second set of parameters corresponds to the global parameters of the simulation. These include the size L of the periodic cubic box, the total mass of the system M_T, the total energy of the system E_T, and the number density x of molecules of species A. These global parameters fix the final thermodynamic state of the system. The next set of parameters corresponds to the transport coefficients D_0, S_0 appearing in Eqs. (A8) and (A9). We assume that the thermal conductivity κ is a constant, independent of the state of the fluid particles. Finally, we have a set of algorithm dependent parameters, h, the radius of the support of the weight function $W(r)$, the number N_T of fluid particles, and the integration time step.

There are many other important parameters in the simulation, but they are all derived from the above parameters. We can further reduce the number of independent parameters by choosing a set of four basic units. In this paper we are considering the following "molecular units:" the unit of length is $L_u=b^{1/D}$ the linear dimension of a molecule, the unit of mass is $M_u=m_0$, the mass of a molecule, the unit of entropy is $S_u=k_B$, the Boltzmann constant, and the unit of temperature is $T_u=T_c$ the critical temperature of the liquid-liquid phase transition. The units of the rest of the variables are trivially obtained from the aforementioned. For instance, the unit of energy will be $E_u=k_B T_c$. We shall further denote dimensionless quantities by the use of starred variables (*).

The input parameters in a simulation run are taken to be the overall number density n_0, the total mass fraction x of species A and the dimensionless box size $L^*=L/b^{1/D}$. The range of possible values are $n_0 \in]0,1[$ and $x \in [0,1]$, otherwise the entropy function and equations of state are ill-defined.

The total number of molecules in the system is given in terms of these input parameters as $N_{\mathrm{mic}}=n_0 V^*$, the total number of A molecules as $N_T^A=xN_{\mathrm{mic}}$, and B molecules as $N_T^B=(1-x)N_{\mathrm{mic}}$, whereas the total dimensionless mass is $M^*=M_T/m_0=N_{\mathrm{mic}}$. The next input parameter is N_T, which is the

TABLE I. Parameters of simulations E_1–E_9.

	E_1	E_2	E_3	E_4	E_5	E_6	E_7	E_8	E_9
N_T	4096	1024	4096	16384	4096	4096	4096	4096	4096
Λ	1	1	1	1	1	1	1	1	1
n_0	0.3	0.3	0.3	0.3	0.3	0.3	0.3	0.3	0.3
L^*	360	180	360	720	360	360	360	360	360
T^*_{init}	1.1	0.6	0.6	0.6	0.7	0.9	0.95	0.8	0.75
x	0.5	0.5	0.5	0.5	0.5	0.5	0.5	0.35	0.7

total number of fluid particles. From this we can compute the typical interparticle distance $\lambda^*=L^*/N_T^{1/D}$, the mass of a fluid particle $m=M_T/N_T$ or in dimensionless units $m^*=N_{\text{mic}}/N_T$, and the total number of molecules per fluid particle $N_0=N_{\text{mic}}/N_T$. In addition the overlapping coefficient $s=h/\lambda$ is also an input that allows us to compute the dimensionless range of the weight function as $h^*=sL^*/N_T^{1/D}$. The chosen value is $s=2.5$ since it insures that the difference between the volume of the box and the sum of all the cell volumes obtained through SPH theory is very small. The definition of the critical temperature in Eq. (28) implies that the dimensionless attraction parameter $a^*=a/(bk_BT_c)$ is fixed to the value $a^*=1/(\Lambda n_0^*)$.

While the Soret-type coefficient S_0 is set to zero for simplicity, the diffusion coefficient and the thermal conductivity coefficient values reflect those of argon, and we also use the atomic mass and atomic size of argon in order to obtain dimensionless values of the used parameters.

In order to solve our set of first order differential equations, we must provide a set of initial conditions for the state variables. For the concentration $x_i(t=0)$ we assign the input concentration x to a particle plus a random contribution within a range of $\pm 0.2\%$ of x, while still keeping $\langle x_i\rangle=x$. This destabilizes slightly the initial state and insures that the system is not set at an artificial computational equilibrium. On the other hand, all temperatures are assigned to T_{init}. The value of T_{init} fixes the global energy content of the system.

V. SIMULATION RESULTS

Nine simulations, whose input parameters are listed in Table I, were carried out until the system reached equilibrium. For instance, E_1 is a simulation of $N_{\text{mic}}=n_0V^*=n_0(L^*)^D=38\,880$ molecules, such that each fluid particle contains $N_0=N_{\text{mic}}/N_T\simeq 9.5$ molecules.

A. Equilibrium phase diagram

Simulations are conducted first in the absence of the surface tension terms, i.e. all $\tilde{\tilde{\phi}}$-related terms are set to zero. As we observe in Fig. 3, the total entropy is a strictly increasing function of time until the equilibrium state is achieved in all the simulations reported. As expected, the entropy increases until it reaches a plateau, therefore complying with the second law of thermodynamics for isolated systems, while the total energy is conserved to machine precision.

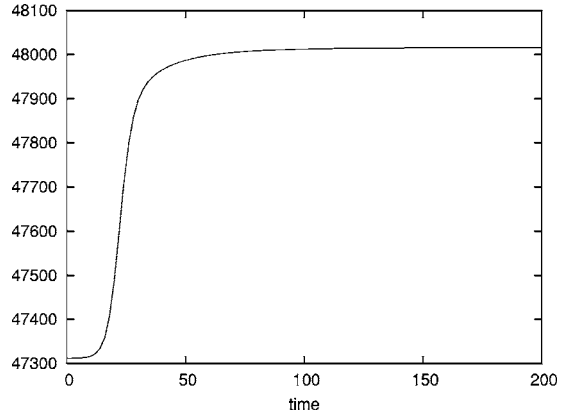

FIG. 3. Total entropy S^* given by Eq. (13) as a function of time. Magnitudes are in molecular units, as described in Sec. IV.

For under-critical situations we expect the values of $\{x_i\}_{\text{eq}}$ to fall into two sets, one which consists of A-rich fluid particles and another, of B-rich particles. This is indeed what happens; the initial distribution of concentrations artificially centered on $x=1/2$ at $t=0$, evolves towards a two-peak distribution, as can be seen in Fig. 4.

When the system is completely phase separated, we can define two quantities, $x_d<0.5$, the average concentration of *dark* (B-rich) particles and $x_l>0.5$ the average concentration of *light* (A-rich) particles. When N_T takes high values, the number of A-rich and B-rich particles are equal, leading to $x_d=1-x_l$. It is important to note that although theory would predict two Dirac delta functions, the outcome of our simulation consists of two very narrow distributions due to the finite number of particles and to the finite simulation time.

One of the observations of these simulations without surface tension, is that neighboring fluid particles can have A- or B-rich phases independent of the state of the given fluid particle. In the simulations, an alternating pattern of A- and B-rich fluid particles arises. The size of the domains of A-rich regions is essentially that of a fluid particle, see Fig. 5.

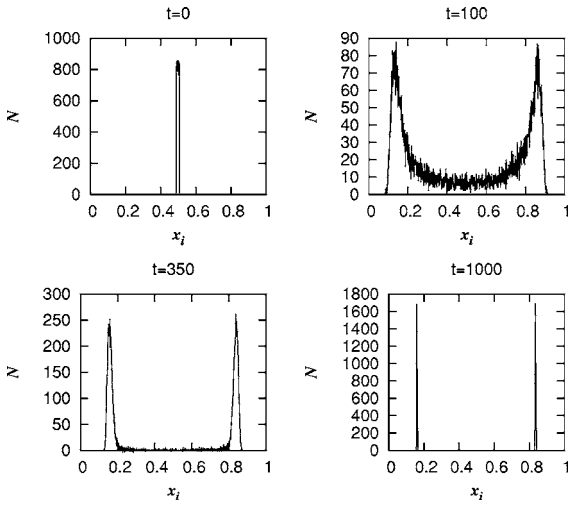

FIG. 4. Histogram of the concentration x_i of the particles at different times for the simulation E_4. Magnitudes are in molecular units, as described in Sec. IV.

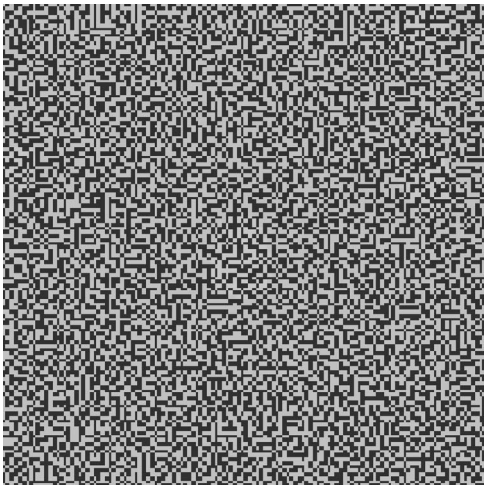

FIG. 5. Phase-separated fluid mixture of E_4; the two-dimensional box is divided in 64×64 particles that either become A- or B-rich. The composition of a cell in species A is indicated in gray scale.

It is also important to remember that although fully phase-separated, the system tends towards a unique equilibrium pressure, a unique equilibrium temperature, and a unique value (equal to zero) of the chemical potential, which was verified in all the conducted experiments.

A very stringent test for the thermodynamic consistency of the model is that the numerical value of the total entropy function evaluated at the equilibrium state $S(x^{\mathrm{eq}})=\Sigma_i S(N_0,\{x_i\}_{\mathrm{eq}},\{U_i\}_{\mathrm{eq}})$ is equal to the entropy function Eq. (20) (which describes the thermodynamic behavior of a fluid particle) evaluated at the global system values of N_{mic},x,E_T. In this way, even though we only specify the thermodynamic behavior of the fluid particles, the full system behaves in a similar thermodynamic way.

We have run two simulations E_{10} and E_{11} which differ in the overall energy of the system, as shown in Table II. Simulation E_{10} is above the critical point and one sees in Fig. 6 that we have a very good agreement between the equilibrium value of the total entropy of the system and the entropy function in Eq. (15) of a fluid particle evaluated at the value of the extensive variables of the whole system.

On the other hand, the simulation E_{11} is clearly subcritical and one observes in Fig. 6 that the simulation points tend to follow a straight line between the two expected peaks. This can be explained in the following way: at equilibrium the fully phase separated system presents $x_d N_T$ B-rich particles and $(1-x_d)N_T$ A-rich particles, all of them at the same equilibrium temperature, and therefore all having the same internal energy [see Eq. (22)], leading to write

TABLE II. Parameters of simulations E_{10} and E_{11}.

	E_{10}	E_{11}
N_T	1024	1024
Λ	1	1
n_0	0.3	0.3
L^*	180	180
T^*_{init}	1.1–1.225	0.6–0.78
x	0.075–0.925	0.075–0.925
E^*_T/N_{mic}	0.6	0.1

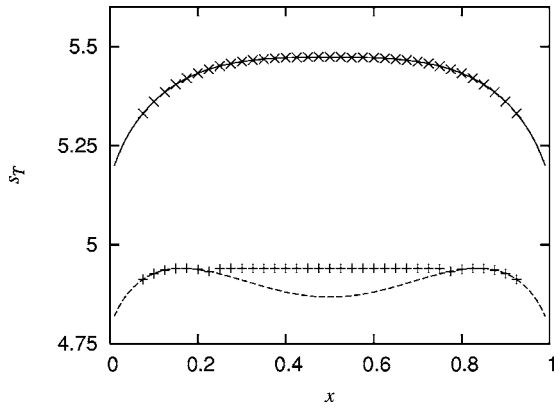

FIG. 6. Equilibrium value of the total entropy per molecule $s_T=S_T/N_{\mathrm{mic}}$ of the system as a function of x for $e_T=E_T/N_{\mathrm{mic}}=0.6$ (plain) with its corresponding simulation results ($\times$) and for $e_T=E_T/N_{\mathrm{mic}}=0.1$ (dashed) with its corresponding simulation results (+). Magnitudes are in molecular units, as described in Sec. IV.

$$
\begin{aligned}
S^*_T &= \sum_i S^*(x_i,U^*_i)\\
&= x_d N_T S^*(x_d,U^*) + (1-x_d)N_T S^*((1-x_d),U^*)\\
&= N_T S^*(x_d,U^*).
\end{aligned}
\tag{31}
$$

The total entropy of the system therefore stays constant regardless of the overall concentration of the system. On the other hand, if the overall concentration x is outside the interval $[x_d,x_l]$, the system does not phase separate and the total entropy of the system follows the theoretical curve, as can be seen in Fig. 6.

Last, we have compared the theoretical and simulated coexistence curves. From Eq. (22), while using the units defined above, one can write the chemical potential as follows ($\Lambda=1$, $\zeta=0$):

$$
\mu^*_i = -T^*_i \ln\frac{1-x_i}{x_i} - 2(2x_i-1), \tag{32}
$$

and the coexistence curve in the T,x space is then given by

$$
T^*_i = \frac{2(2x_i-1)}{\ln\frac{x_i}{1-x_i}}. \tag{33}
$$

In Fig. 7 we plot the equilibrium temperature $T^{\mathrm{eq}}<1$ as a function of the concentrations x_d and x_l for the simulations $E_{2,\ldots,9}$. We also perform another simulation, E_{12}, that shares its parameters with E_3, but we vary the initial temperature from 0.35 until 0.999. We indeed observe that our code converges towards the expected values of x_d and x_l. In all cases the agreement between theory and simulation results is excellent. It is interesting to remark that E_2,E_3, and E_4 are very similar in the sense that N_0 (the number of molecules per particle) is the same for all, but the size of E_4 is a system 4 times bigger than E_3 itself 4 times bigger than E_2, leading to

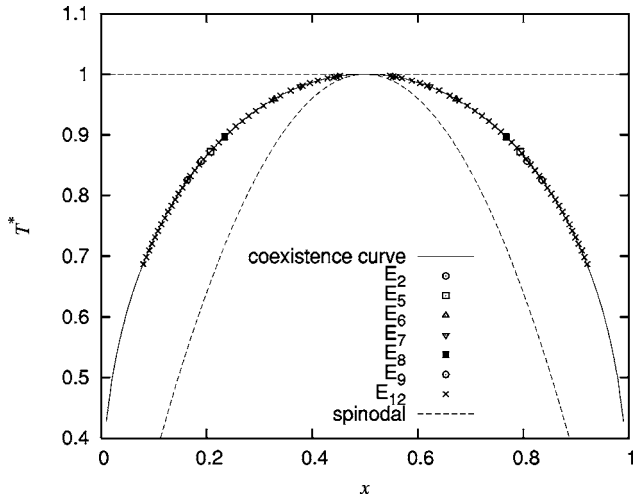

FIG. 7. The concentrations of the coexisting phases at different temperatures. The solid line stands for the theoretical coexistence curve, while the symbols are results from the numerical simulations. Magnitudes are in molecular units, as described in Sec. IV.

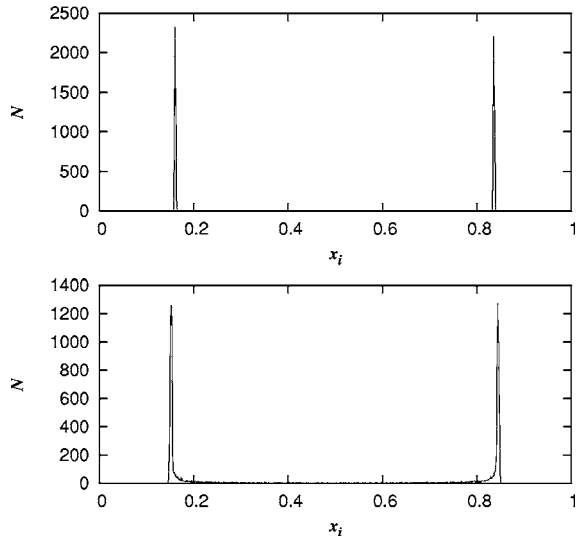

FIG. 8. Histogram of the concentration x_i of the particles in the case of no surface tension (above), and in the case where surface tension terms are included (under). Parameters are those of E_3.

the conclusion that the size of the sample for a given physical experiment is irrelevant regarding the outcome of the simulations.

We plot also in Fig. 7 the spinodal curve which is the metastability limit of the binary mixture. The mixture becomes unstable inside the spinodal (leading to full phase separation) while it is metastable between the coexistence and the spinodal curves. Its locus is given by the change of sign of the curvature of the entropy, i.e., where $\partial\mu/\partial x_i^{\mathrm{eq}}=0$ at constant energy. When simulations were initially started in between the two curves phase separation occurred or not depending on the randomness on the initial values of x_i.

B. Non-equilibrium phase results

When we introduce the surface tension terms, there is an energy cost for having neighbor particles with different concentrations. The system now segregates into regions of A- and B-rich mass fraction separated by smooth interfaces. In Fig. 8 we compare the distribution of mass fraction for the simulation E_3 with and without the surface tension terms. The two equilibrium values of the mass fraction have not changed appreciably, but the width of the distribution is larger when surface tension is included. The width of the distribution of mass fraction is a reflection of the smooth transition occurring in the interfacial regions. It is quite remarkable that the introduction of surface tension does not change the phase diagram (i.e., the location of the peaks in Fig. 8). However for this to happen, it is necessary that the size of the interfacial region separating A and B regions is small compared with the total size of the system. Because the interface width grows as we approach the critical point, system size dependences are observed near the critical point.

We explore the effect of the magnitude of the surface tension effects by setting a coefficient q in front of every surface tension term in the equations (i.e., the $\tilde{\phi}$ terms), and look at the system for different values of $q \in [0:1]$. We run a simulation with 256×256 particles, with $T_{\mathrm{init}}=0.6$ for a time $t=300$ dimensionless time units. The system does not reach the equilibrium state in this time. In Fig. 9 we present the distribution of mass fraction for five values of q, while in Fig. 10 snapshots of the system at this time are presented for different values of q. We observe that the larger the intensity of the surface tension, the wider the peaks of the distribution of mass fraction. This is a reflection that the domains are larger the larger is the intensity of the surface tension and, in addition, the interfacial width is larger the larger is the intensity of the surface tension.

In order to illustrate that the model can tackle more complex and interesting situations, we set our system at an initial upper-critical temperature of 1.3 and impose a gradient of temperature as follows: all particles in the middle horizontal axis are suddenly cooled down to a temperature of 0.5, while all particles at upper horizontal border of the box are maintained at the initial temperature 1.3. This is achieved by means of an extra term in the $\dot{U}_i$ equation,

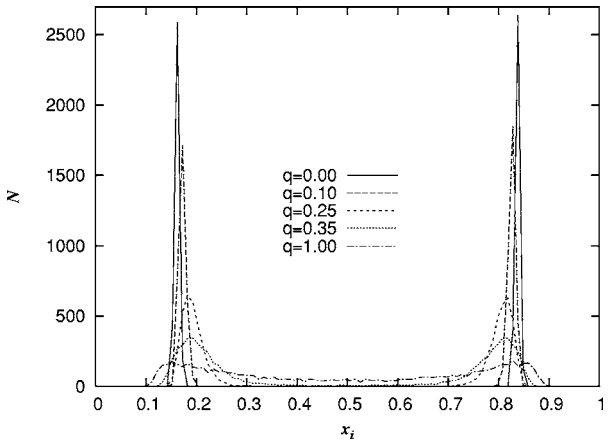

FIG. 9. Histogram of the concentration x_i of the particles at time $t=300$ for different values of the coefficient q.

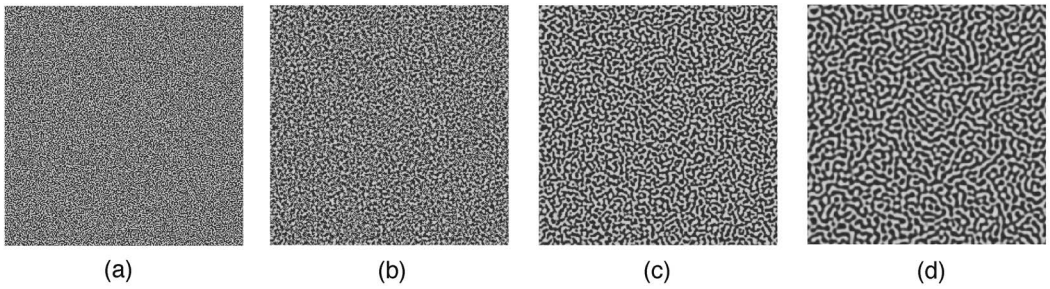

FIG. 10. Effect of the intensity of the surface tension term on the patterns of spinodal decomposition of otherwise identical samples, $q=0$ (a), $q=0.35$ (b), $q=0.5$ (c), $q=1$ (d).

$$-\kappa_g(T_i^* - \mathcal{T}_i), \tag{34}$$

where κ_g is the heat conductivity of the hypothetical cooling system lying underneath our system, and $\mathcal{T}_i$ is the temperature desired at particle i.

We present in Fig. 11 a time sequence of the phase separation under a temperature gradient. The sudden cooling of the central line produces a space and time varying temperature field. The critical isotherms are two horizontal lines that move from the center outwards towards the top and bottom of the system. At the steady state they are located at $y \approx 0.3$ and $y \approx -0.3$. In between these two isotherms the temperature is under-critical and the system phase separates. Initially the domains have a typical length scale characteristic of spinodal decomposition and have no particular orientation. As time proceeds, though, the domains align parallel to the temperature gradient with a characteristic length scale. The blurred edges near to the hot bath lines indicate the position of the critical isotherms. Similar simulations of mixtures in the presence of temperature gradients have been reported by Jasnow and Viñals [25]. Note, however that in counter-distinction with the present work, the simulations in Ref. [25] are those on a model in which the temperature is not dynamically coupled to the concentration field.

Another experiment was performed; we set the system at initial temperature 1.01 but set $\mathcal{T}_i=0.5$ for the particle in the middle of the system by the same means described here above. This would mimic the effect of inserting a cold needle in an upper-critical mixture. It results first in a succession of concentric rings that ultimately evolve towards a unique drop formed in the middle of the system; see Fig. 12. The initial mass fraction is $x=0.5$, but we have also experimented with other concentrations leading to square symmetrical arrangements (due to the periodic boundary conditions) of many droplets of the minority phase [32]. These droplets are expected to merge in an extremely long time scale in a one single droplet.

Note that interesting and intriguing patterns can have far reaching technological applications. For if the binary mixture phase can be further solidified through rapid quenching, the resulting material properties of the structures can have rather different mechanical and structural properties, different from the originally mixed systems. The theoretical understanding

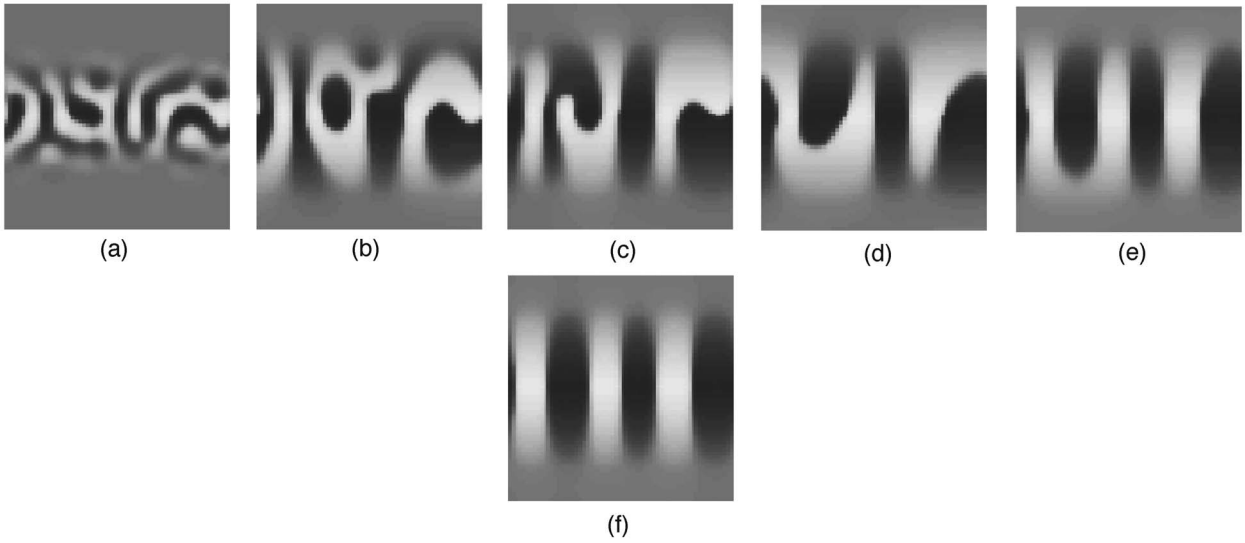

FIG. 11. Evolution of an upper-critical binary mixture at $T^*_{\text{init}}=1.01$ when two horizontal lines are suddenly brought to temperatures $T^*_{\text{hot}}=1.3$ (in the middle of the sample) and $T^*_{\text{cold}}=0.5$ (at the bottom/top of the sample, which has periodic boundary conditions) thus creating a two-ramp temperature gradient. The different pictures correspond to times (a) $t^*=400$, (b) $t^*=3200$, (c) $t^*=7400$, (d) $t^*=13\,000$, (e) $t^*=19\,600$, (f) $t^*=75\,000$ ($x=0.5$, $N_T=4096$, $L^*=360$.)

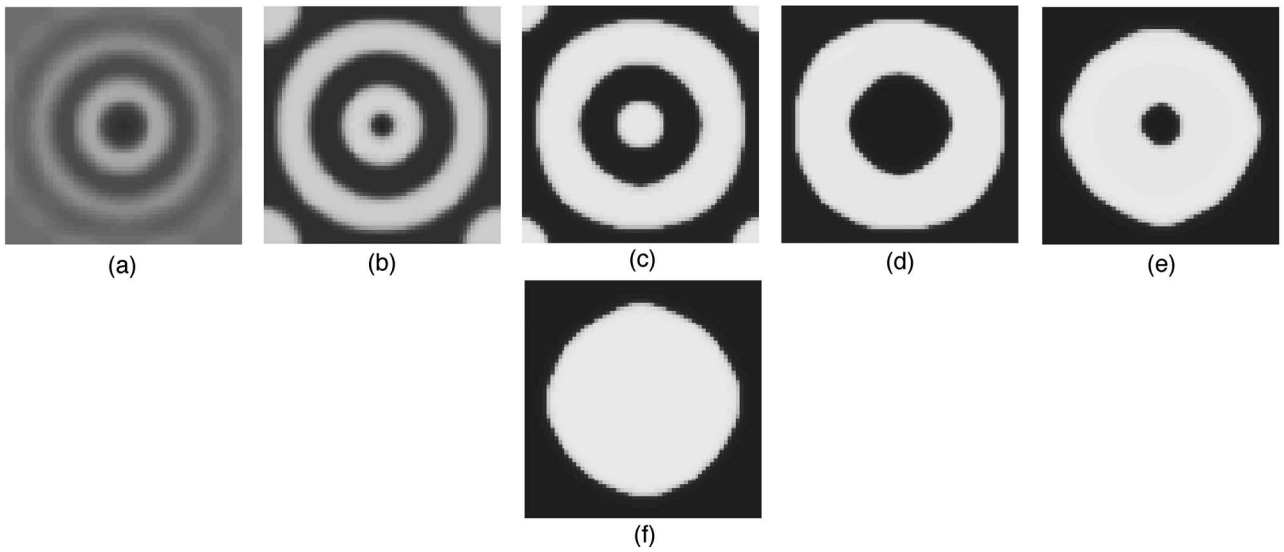

FIG. 12. Evolution of an upper-critical binary mixture at $T^*_{\text{init}}=1.01$ when single "needle" at the middle of the sample is maintained at an under-critical temperature $T^*_{\text{cold}}=0.6$. The different pictures correspond to times (a) $t^*=2000$, (b) $t^*=10\,000$, (c) $t^*=30\,000$, (d) $t^*=60\,000$, (e) $t^*=200\,000$, (f) $t^*=300\,000$ ($x=0.5$, $N_T=4096$, $L^*=360$.)

and control of these patterns in nonisothermal situations can open the way to the construction of techniques for designing new composite polymer materials with valuable properties.

VI. DISCUSSION

In this paper, we have validated through numerical simulations the SPH model for phase separating mixtures in the simplest nontrivial case. Viscous processes are neglected and only mass and energy diffusive processes take place. We also restricted ourselves to the case of a binary mixture that can exhibit only liquid-liquid phase separation. The model satisfies the first and second law of thermodynamics; the total energy of the system is conserved and the total entropy of the system is an increasing function of time. The van der Waals thermodynamic behavior is recovered by the simulations when they reach the equilibrium state. Below the critical temperature the mixture phase separates and regions of A-rich or B-rich regions appear separated by diffuse interfaces. The role of the strength of the surface tension has been qualitatively investigated in the dynamics of the formation of domains. We observe that higher surface tension implies slower dynamics along with larger domains and interface widths.

We have observed that near the critical point, when the interfaces have a large width, the simulated coexistence curve departs slightly from the van der Waals equation of state. This may be attributed to the difficulty of having well-defined bulk values for the mass fraction of each phase through the system. For system sizes much larger than the interfacial width, regions with well-defined bulk values exist and the departure from the van der Waals coexistence curve should vanish. On the other hand, within the critical region thermal fluctuations are enhanced. Our model does not include thermal fluctuations but they could be introduced easily. We expect that when thermal fluctuations are included in the model, we should observe again deviations of the measured coexistence curve and the van der Waals prediction, even in the limit of very large system sizes. In particular, we expect to obtain nonmean field exponents for the flatness of the coexistence curve. In order to validate this conjecture, one should run very large simulations in order to account for finite size effects and the critical slowing down which is characteristic of the dynamics near the critical point. We leave this study for future work.

In this preliminary work, we have investigated qualitatively the effect of imposing nonhomogeneous temperature distributions on the dynamics of the phase separation. Temperature inhomogeneities created either by walls at different temperatures or local sinks of energy lead to very interesting pattern formation with complex dynamics that deserve future investigation.

The discrete fluid particle model that we have presented in this paper allows one to describe liquid-liquid phase transition but not gas-liquid transitions that, in principle, are accommodated by the more general model in Ref. [27]. The reason is that the number density of every fluid particle is fixed in the simulation. The particles do not move, their volume is fixed, and the mass of a fluid particle is constant. We expect that when the particles are allowed to move according to the dynamic equations presented in Ref. [11], in the region of thermodynamic parameters where the van der Waals equation of state predicts gas-liquid coexistence, the fluid particles will distribute in space in such a way to produce liquid regions of high density (the fluid particles all have the same mass or N_0, but they are packed together so their volumes are small) coexisting with gaslike sparse distributions of fluid particles. In particular, we expect that for a simple fluid with $x_i=1$ the model allows one to describe the usual van der Waals gas-liquid transition. Simulations of coexisting liquid droplets with its vapor have been conducted in Ref. [31] with the SPH method. However, surface tension was treated in a rather unconventional way by using a weight function with

different ranges. In counter-distinction to our model where the coefficients $c_{\alpha\beta}$ control surface tension, there is no direct control to the surface tension in the model of Ref. [31]. We plan to address this issue in a future work.

ACKNOWLEDGMENTS

This research has been partially supported by the Spanish MCYT under Grant No. BFM2001-0290 and the European Community under Project No. ICOPAC.

APPENDIX

In this appendix, we motivate the functional dependence of the transport coefficients in Eqs. (14). In Ref. [11] we presented Green-Kubo expressions for the diffusion transport coefficients in the form

$$D_i^{\alpha\beta} = \frac{1}{2k_B T_i}\frac{1}{\mathcal{V}_i}\int_{-\infty}^{\infty} dt \frac{1}{3}\langle \mathbf{V}^\alpha \cdot \mathbf{V}^\beta(t)\rangle_i^{\mathrm{eq}}, \tag{A1}$$

where T_i is the temperature, $\mathcal{V}_i$ is the volume of the fluid particle and the average velocity of species α is defined as

$$\mathbf{V}^\alpha = \sum_{i_\alpha}^{N^\alpha} \mathbf{v}_{i_\alpha}, \tag{A2}$$

where $\mathbf{v}_{i_\alpha}$ is the velocity of the ith molecule of species α within the ith fluid particle. The equilibrium average $\langle\cdots\rangle_i^{\mathrm{eq}}$ is one of molecular nature, that is to say, with an ensemble which is microcanonical in the total energy and total momentum of the fluid particle. The total momentum of the fluid particle is zero in this equilibrium ensemble. As a consequence, restrictions (1) apply because if we multiply $D_i^{\alpha\beta}$ by m_α and sum over species we get inside the equilibrium average the term $\Sigma_\alpha m_\alpha \Sigma_{i_\alpha}^{N^\alpha} \mathbf{v}_{i_\alpha}$ which is the total momentum of the system. Because the equilibrium average is microcanonical in the momentum with zero momentum, the average vanishes, leading to (1). In a binary mixture, we must only consider a single diffusion coefficient. Starting with D^{AA}, we present an estimate of this diffusion coefficient based on the overall amplitude of the velocity correlation at time $t=0$. At this initial time, it is possible to compute the equilibrium average with the result

$$\frac{1}{3}\langle \mathbf{V}^A \cdot \mathbf{V}^A\rangle_i^{\mathrm{eq}} = N_i^A \frac{k_B T_i}{m^A}. \tag{A3}$$

Therefore we have $D_i^{AA} = (n_i^A/m_A)\tau(n_i^A, n_i^B, T_i)$ where $n_i^\alpha = N_i^\alpha/\mathcal{V}_i$. In addition to this we have introduced the correlation time of the velocity

$$\tau^A(n_i^A, n_i^B, T_i) = \frac{1}{2}\int_{-\infty}^{\infty} dt \frac{\langle \mathbf{V}^A \cdot \mathbf{V}^A(t)\rangle_i^{\mathrm{eq}}}{\langle \mathbf{V}^A \cdot \mathbf{V}^A\rangle_i^{\mathrm{eq}}}. \tag{A4}$$

This is the correlation time of the average velocity of species A. In principle, this correlation time depends on the thermodynamic state of the fluid particle. We would like to have a simple model for this correlation time as a function of the state of the fluid particle. Note that the restriction (1) implies the following relationship between τ^A and τ^B,

$$m_A n_i^A \tau^A(n_i^A, n_i^B, T_i) = m_B n_i^B \tau^B(n_i^A, n_i^B, T_i). \tag{A5}$$

This equation clearly shows that $\tau^A(n_i^A, n_i^B, T_i)$ and $\tau^B(n_i^A, n_i^B, T_i)$ must depend on n^A, n^B, otherwise (A5) cannot generally be fulfilled. The simplest possible assumption would be then to take $\tau^A = n^B m_B c$ and $\tau^B = n^A m_A c$, where c is a constant, independent of the thermodynamic state. Therefore, we will assume the following model for the diffusion coefficient:

$$D^{AA} = n^A n^B \frac{m_B}{m_A} c,$$

$$D^{BB} = n^A n^B \frac{m_A}{m_B} c, \tag{A6}$$

or, in terms of the variables N_0, x and for the simple case that the molecules have the same mass $m_A = m_B$,

$$D^{AA} = D^{BB} = n_0^2 x(1-x)c. \tag{A7}$$

The corresponding transport coefficient D_i introduced in (2) and appearing in the dynamic equations (4) and (5) will take the form of

$$D_i = D_0 x_i(1-x_i), \tag{A8}$$

where $D_0 = m_0^2 n_0 c$ is a constant. Note that the diffusionlike transport coefficient vanishes in the limits of simple A, B fluids, where $x = 1, 0$.

Although a simple argument like the one presented above for the diffusionlike coefficient D_i is not easily available for the cross coefficient S_i, we assume that the functional form of S_i is also of the form

$$S_i = S_0 x_i(1-x_i), \tag{A9}$$

where S_0 is a constant.

[1] J. W. Cahn and J. E. Hilliard, J. Chem. Phys. **28**, 258 (1958).
[2] S. M. Allenand and J. W. Cahn, Acta Metall. **27**, 1085 (1979).
[3] S. Bastea and J. L. Lebowitz, Phys. Rev. Lett. **78**, 3499 (1997).
[4] S. Bastea, R. Esposito, J. L. Lebowitz, and R. Marra, J. Stat. Phys. **101**, 1087 (2000).
[5] L. Antanovskii, Phys. Fluids **7**, 747 (1994).
[6] J. Lowengrub and L. Truskinovsky, Proc. R. Soc. London, Ser. A **454**, 2617 (1998).
[7] P. Papatzacos, Phys. Scr. **61**, 349 (2000).

[8] O. Dinariyev, J. Appl. Math. Mech. **65**, 471 (2001).
[9] D. M. Anderson, G. B. McFadden, and A. A. Wheeler, Annu. Rev. Fluid Mech. **30**, 139 (1998).
[10] P. Español, J. Chem. Phys. **115**, 5392 (2001).
[11] P. Español and C. Thieulot, J. Chem. Phys. **118**, 9109 (2003).
[12] B. Nadiga and S. Zaleski, Eur. J. Mech. B/Fluids **15**, 885 (1996).
[13] D. Jacqmin, J. Comput. Phys. **155**, 96 (1999).
[14] V. M. Kendon, J.-C. Desplat, P. Bladon, and M. E. Cates, Phys. Rev. Lett. **83**, 576 (1999).
[15] V. M. Kendon, M. E. Cates, J.-C. Desplat, I. Pagonabarraga, and P. Bladon, J. Fluid Mech. **440**, 147 (2001).
[16] P. V. Coveney and K. E. Novik, Phys. Rev. E **54**, 5134 (1996).
[17] P. B. Warren, Phys. Rev. Lett. **87**, 225702 (2001).
[18] I. Pagonabarraga and D. Frenkel, J. Chem. Phys. **115**, 5015 (2001).
[19] G. Leptoukh, B. Strickland, and C. Roland, Phys. Rev. Lett. **74**, 3636 (1995).
[20] H. Furukawa, Phys. Rev. E **55**, 1150 (1997).
[21] I. M. Lifshitz and V. V. Slyozov, J. Phys. Chem. Solids **19**, 35 (1961).
[22] M. Grant and K. R. Elder, Phys. Rev. Lett. **82**, 14 (1999).
[23] J. M. Yeomans, Annu. Rev. Comput. Phys. **7**, 61 (1999).
[24] G. Gonnella, E. Orlandini, and J. M. Yeomans, Phys. Rev. Lett. **78**, 1695 (1997).
[25] D. Jasnow and J. Viñals, Phys. Fluids **8**, 660 (1996).
[26] H. T. Davis, *Statistical Mechanics of Phases, Interfaces and Thin Films* (Wiley-VCH, New York, 1996).
[27] C. Thieulot, L. P. B. M. Janssen, and P. Español, preceding paper, Phys. Rev. E **72**, 016713 (2005).
[28] P. H. Konynenburg and R. L. Scott, Philos. Trans. R. Soc. London, Ser. A **298**, 495 (1980).
[29] H. B. Callen, *Thermodynamics* (Wiley, New York, 1960).
[30] J. J. Monaghan, Annu. Rev. Astron. Astrophys. **30**, 543 (1992).
[31] S. Nugent and H. A. Posch, Phys. Rev. E **62**, 4968 (2000).
[32] C. Thieulot and P. Español, Comput. Phys. Commun. (to be published).